FRONTIERS OF PHYSICS

RESEARCH ARTICLE
Volume 17 / Issue 6 / 63501 / 2022

Bioinspired mineral MXene hydrogels for tensile strain sensing and radionuclide adsorption applications

Xin Li[1,2], Guangcun Shan[1,2,†], Ruguang Ma[2,4], Chan-Hung Shek[2], Hongbin Zhao[3,‡], Seeram Ramakrishna[5]

1 School of Instrumentation Science and Opto-electronics Engineering, Beihang University, Beijing 100191, China
2 Department of Materials Science and Engineering, City University of Hong Kong, Kowloon Tong, Hong Kong SAR, China
3 State Key Laboratory of Advanced Materials for Smart Sensing, General Research Institute for Nonferrous Metals, Beijing 100088, China
4 Institute of Materials Science and Devices, Suzhou University of Science and Technology, Suzhou 215009, China
5 Department of Mechanical Engineering & Circular Economy Taskforce, National University of Singapore, Singapore 119077, Singapore
Corresponding authors. E-mail: †gshan2-c@my.cityu.edu.hk, ‡zhaohongbin@grinm.com
Received May 4, 2022; accepted May 27, 2022

ABSTRACT

MXene-based hydrogels have drawn considerable attention as flexible and wearable sensors. However, the application of MXene-based hydrogels after sensing failure has rarely been investigated, which is of great significance for expanding their engineering application. In this work, multifunctional mineral MXene hydrogels (MMHs) were synthesized via a simple method inspired by biomineralization. The prepared MMHs were stretchable, self-healable and conductive, and can be used to fabricate wearable tensile strain sensors showing a super-wide sensing range with excellent sensitivity. MMHs-based strain sensors were designed to be directly attached to the skin surface to detect tiny and large human motions. In addition, with the advantages of a large specific area, excellent hydrophilicity and abundant active adsorption sites for MXene nanosheets and hydrogels, dehydrated MMHs were used as highly efficient adsorbents for the removal of strontium ions from aqueous solutions. This work shows the great potential of MXene in promoting the development of next-generation functional materials.

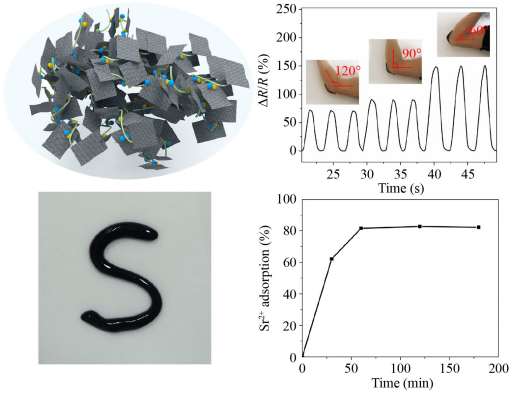

Keywords MXene, hydrogel, flexible sensor, adsorption

1 Introduction

Through biomineralization [1, 2], organisms could generate inorganic mineral materials with unique structures and functions, such as bones, shells, and teeth. The formation of biominerals with different shapes or structures is mainly the result of irreversible crystallization of amorphous precursors, such as amorphous calcium carbonate (ACC) [3, 4]. Inspired by biomineralization, Sun *et al.* [5] developed reapable and self-healable mineral hydrogels by stabilizing ACC with polymer additives, polyacrylic acid (PAA). The prepared ACC-PAA hybrid hydrogels were called "mineral plastics", which are environmentally

* Special Topic: MXene and Its Applications (Eds.: Qing Huang, JuHan Lee & Guangcun Shan).

Higher Education Press

https://doi.org/10.1007/s11467-022-1181-2

friendly and recyclable. With cross-linked hydrophilic polymer chains, hydrogels exhibit three-dimensional (3D) architecture that is highly stretchable, self-healing and even biocompatible [6–8]. Hydrogels can be used as an excellent carrier or framework for functional composites. Developing conductive hydrogels based on conductive mediums has become a research hotspot in recent years. Conductive hydrogels have shown great potential in flexible and stretchable sensors [9–11], electronic skins [12, 13], supercapacitors [14, 15], etc.

MXene is a new family member of two-dimensional (2D) materials, which refers to 2D early transition metal carbide or carbonitride [16, 17]. With the free electrons of the transition metal layer as carriers, MXene shows metal-like conductivity. MXene has been demonstrated to have potential in sensors [18–20], energy storage [21], electromagnetic-wave absorption [22], etc. The surface of MXene prepared by chemical liquid phase etching is usually rich in groups such as –OH, –O and –F, making it strongly hydrophilic and possible to composite with hydrogels [23, 24]. Conductive networks would be formed in MXene-based hydrogel composites, whose resistance would change under external force. Therefore, MXene-based hydrogels could be used as sensing materials in flexible pressure or strain sensors [25–29]. The three-dimensional porous structure of hydrogels would make up for the shortcomings of the planar brittleness of 2D MXene and benefits the performance of the prepared flexible sensors.

However, MXene-based hydrogels can only serve as sensing materials in a water-rich state. In the dry state, MXene-based hydrogels become hard and brittle and lose their sensing ability. Studies on the functional application of dehydrated MXene-based hydrogels would help improve their engineering application value. Interestingly, layered MXene [30–33] and porous hydrogels [34–38] both showed large specific area, excellent hydrophilicity and abundant active adsorption sites, which indicated their promising application in adsorbents. Furthermore, it has been demonstrated that MXene-based adsorbents showed good radiation resistance [39, 40]. Therefore, in addition to strain sensitivity, MXene-based hydrogels are expected to have excellent adsorption capacity for heavy metal ions and be promising adsorbents for efficient radionuclide removal from aqueous solutions and even from seawater.

By introducing MXene, Liu *et al.* [41] developed a porous MXene-based composite aerogel, which showed sensitive piezoresistive sensing performance and high adsorption capacity for various oils and organic solvents. In this work, conductive, stretchable, self-healable and porous mineral MXene hydrogels (MMHs) consisting of MXene, PAA and ACC were synthesized via a facile preparation procedure inspired by biomineralization. The prepared MMHs showed a dynamic cross-linked network attributed to the chelation between calcium ions (Ca^{2+}) and reactive functional groups in both PAA polymer and MXene nanosheets. MMHs were studied as tensile strain sensors, which showed a wide sensing range with acceptable sensitivity to monitor kinds of human motions, for example, joints bending and swallowing. In addition, it was found that dehydrated MMHs were no longer strain sensitive but can be used as highly efficient adsorbents to remove Sr^{2+} from aqueous solutions.

2 Experimental

2.1 Preparation of MMHs

PAA ($M_w \approx 100\ 000$ g/mol, 35wt.% in H_2O) was sourced from Sigma-Aldrich Co., Ltd. Sodium Carbonate ($CaCl_2$, ≥96.0%) and Calcium Chloride (Na_2CO_3, ≥99.8%) were purchased from Shanghai Titan Scientific Co., Ltd. Titanium Carbide ($Ti_3C_2Ti_x$) was provided by Jilin 11 Technology Co., Ltd. Layered MXene was prepared by sonicating with an ice bath for 30 min. During the ultrasound process, the solution was held in a sealed glass vial and filled with argon.

First, PAA (0.2 M) and $CaCl_2$ (0.2 M) were added into MXene dispersion (0.6 mg/mL) sequentially with vigorously magnetic stirring at 25 ℃ for 15 min. Second, Na_2CO_3 (0.1 M) was slowly injected into the black mixture using a syringe pump with a speed of 80 mL/h. Finally, with the addition of Na_2CO_3 and continuous stirring, the black hydrogel was formed around the stirring bar. At the same time, the solution faded black and became a turbid white liquid. The hydrogel was collected and washed several times using deionized water.

2.2 Fabrication of strain sensor

MMHs were reshaped into strips using 3D printed resin molds and then equipped with two silver wires at each end as electrodes. The strip-shaped MMHs were sandwiched between two layers of stretchable and insulating tape (VHB 4905, 3M). The sandwich strain sensor can be easily attached to the surface of the test objects with the adhesiveness of the tapes.

In addition, MMHs were directly injected into a silicone tube with a standard 1.5 mL syringe to fabricate the fiber strain sensor. Two silver wires were also inserted as electrodes, and the two ends of the silicone tube were sealed with glue.

2.3 Characterization

MMHs were freeze-dried for 12 hours, and the product was used for characterizations. The morphology of MMHs was studied using field emission scanning electron

microscopy (SEM, Zeiss Supra55). Fourier-transform infrared spectroscopy (FT-IR) spectroscopy was carried out on an FT-IR spectrometer (IS10, Nicolet). X-ray photoelectron spectroscopy (XPS) was acquired by an X-ray photoelectron spectrometer (ESCALAB 250Xi, Thermo Scientific) with Al Kα X-rays ($h\nu$ = 1486.6 eV) radiation.

2.4 Strain sensing and batch sorption experiments

Strain sensing tests were carried out by using a Keithley 4200A-SCS parameter analyzer and a universal tensile testing machine. The tensile testing machine was programmed to make the sensor under different deformations and record the strain parameters over time. At the same time, the Keithley 4200 was set to supply a constant voltage of 5V between the two ends of strain sensors and record the current in real-time. As a result, the resistance variation in response to strain changes can be calculated using Ohm's law. Baseline correction and filtering were applied to the small tensile strain range data.

The MHHs after strain sensing experiments were used for batch sorption experiments to evaluate their adsorption capability for Sr^{2+} ions. Sr^{2+} aqueous solutions were prepared by mixing $SrCl_2$ aqueous solution and deionized water. To investigate the kinetics of the adsorption process, MMHs were added into Sr^{2+} aqueous solution in sealed glass tubes on a thermostat rotary shaker. After the pre-designed reaction time, aqueous solution samples were obtained by centrifuging, and the remaining Sr^{2+} concentration was measured by inductively coupled plasma mass spectrometry (ICP-MS). The removal efficiency (RE) and equilibrium adsorption capacity (q_e) were calculated by

$$RE = \frac{C_0 - C_e}{C_0} \times 100\%, \tag{1}$$

$$q_e = \frac{(C_0 - C_e)\,V}{m}, \tag{2}$$

where C_0 (mg/L) and C_e (mg/L) are the Sr^{2+} concentration in the aqueous solution before and after adsorption, respectively; m (g) is the mass of the adsorbent, and V (L) is the volume of the applied Sr^{2+} aqueous solution. C_0 = 100 mg/L, m = 5 mg, V = 5 mL.

3 Results and discussion

The cross-linked structure of MMHs is shown in Fig. 1(a), which schematically illustrates the chelation between Ca^{2+} and reactive functional groups in both PPA polymer and MXene nanosheets. Figure 1(b) is a SEM image of freeze-dried MMHs, showing typical cross-linked and porous architecture like other mineral hydrogels [10, 11, 42, 43]. The excellent electromechanical properties of MMHs could be attributed to the chelation between Ca^{2+} and COO^- from PAA and MXene, as indicated in the FT-IR spectra in Fig. 1(c). There is an obvious peak at 1704 cm^{-1} (v(COOH)) in the spectrum of PAA. However, that peak was weakened a lot, and a new peak appeared at 1548 cm^{-1} ($v(COO^-)$) in the spectrums of ACC-PAA and MMHs, which indicated the chelation. All the FT-IR spectrums are normalized by the strongest peak value of each other. The existence of amorphous calcium carbonate (ACC) could be evaluated by three characteristic peaks located at 1455–1480/1396–1427 cm^{-1} (double v_3), 1065–1075 cm^{-1} (v_1) and 862–873 cm^{-1} (v_2) [44]. In Fig. 1(c), the vibrational bands of v_3 (1406 cm^{-1}) can be obviously observed.

The chemical composition of MMHs was characterized by XPS. The XPS survey spectra of MMHs sample is shown in Fig. 1(d). The peaks of F 1s, O 1s, Ti 2p, Ca 2p and C 1s could be clearly identified at around 685, 532, 456, 347 and 285 eV, respectively. The presence of a small amount of fluorine was due to the incomplete reaction during the preparation of MXene. Figure S1(a) in the Supplementary shows the Ca 2p core-level XPS spectrum of MMHs, which was fitted into two peaks corresponding to Ca $2P_{1/2}$ (350.9 eV) and $Ca2P_{3/2}$ (347.4 eV) with the area percentages of 32% and 68%, respectively. The Ti 2p core-level XPS spectrum of MMHs was fitted into four pairs of peaks (Ti $2p_{3/2}$ and Ti $2p_{1/2}$) with a fixed area ratio of 2:1, as shown in Fig. S1(b) (Supplementary). According to the fitting result, the 4 Ti $2p_{3/2}$ peaks can be assigned to Ti-C (454.8 eV), Ti(Ⅱ) suboxides or hydroxides (456.0 eV), Ti(III) suboxides or hydroxides (457.3 eV), and Ti(IV) oxides (458.8 eV) [45] with the area percentages of 43%, 31%, 18%, and 8%, respectively. In Supplementary Fig. S1(c), the C1s spectrum was fitted into two peaks corresponding to C–C (284.8 eV), C–O–C (286.1 eV), C(O)O (289.1 eV), C=O (288.6 eV) and C–Ti (281.5 eV), respectively, with the area percentages of 68%, 5%, 7%, 18% and 2%, respectively, which indicated the chelation again.

The addition of MXene significantly improved the mechanical properties of new hydrogels compared to ACC-PAA hydrogel, which could be attributed to the stronger chelation and the outstanding mechanical properties of MXene. Figure 1(e) shows that the prepared MMHs could be easily reshaped into different shapes, indicating their great potential in flexible electronics. All shapes shown in Fig. 1(e) were manipulated from the same piece of MMHs at room temperature. In other words, the prepared MMHs is self-healable.

Figure 1(e) and Movie S1 in the Supplementary show that MMHs are highly stretchable, but this kind of large deformation is not self-reversible. To fabricate a flexible strain sensor, MMHs were reshaped into thin strips and sandwiched in two layers of VHB tapes, as shown in Fig. 2(a). VHB tapes could restore MMHs after large tensile

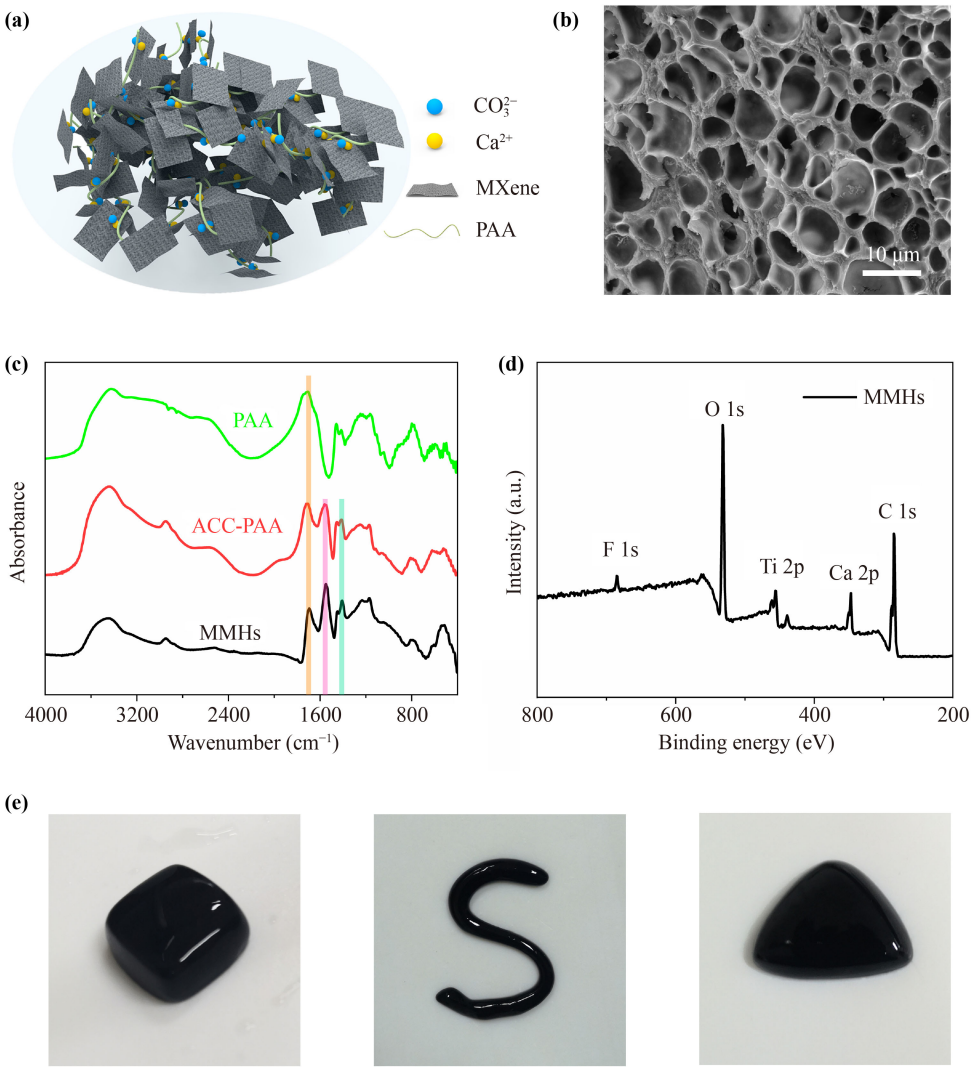

Fig. 1 **(a)** Schematic illustration of the microstructure of MMHs. **(b)** SEM image of freeze-dried MMHs sample. **(c)** FT-IR spectra of PAA, ACC-PAA and MMHs. **(d)** XPS survey spectra of MMHs. **(e)** MMHs were manipulated into different kinds of shapes.

deformation to the original state while playing the role of insulating packaging. It is well known that the conductivity of MXene is excellent; thus, the resistivity of MMHs will be greatly improved by introducing MXene. According to the electrical resistance formula of a conductor, $R = \rho l/A$, where ρ, l and A are the resistivity, length and cross-section area, respectively, the resistance of a conductor is directly and inversely proportional to its length and cross-section area, respectively. Under external tensile strain, the length and cross-section area of MMHs will absolutely become longer and smaller than in the static state, which means the electron transfer pathway will be longer and more crowded so that the resistance will increase. Therefore, highly stretchable and conductive MMHs would be a good sensing material for resistive strain sensors. Using a universal tensile testing machine, different levels of continuously changing mechanical strain, 1%–600%, were applied to the sandwich strain sensor with a constant frequency of 0.05 Hz. The corresponding electrical resistance was measured, and the resistance variation was calculated by $\Delta R/R_0 = (R - R_0)/R_0$, where R_0 is the initial resistance (strain $\varepsilon = 0$ %) and R is the real-time resistance at different strain. As shown in Figs. 2(b) and (c), the resistance of the strain sensor always maintained linear, symmetric and periodic change under a dynamic strain range. All peaks correspond to the maximum strain, and all valleys correspond to the minimum strain ($\varepsilon = 0$ %). The sensitivity of the strain sensor was defined as gauge factor (GF), which is described by

$$GF = \frac{\Delta R/R_0}{\Delta L/L_0} = \frac{\Delta R/R_0}{\varepsilon}, \tag{3}$$

where $\Delta L/L_0$ denotes the length variation of the strain sensor under applied mechanical strain, which is usually described as ε. Five repetitions of each tensile experiment

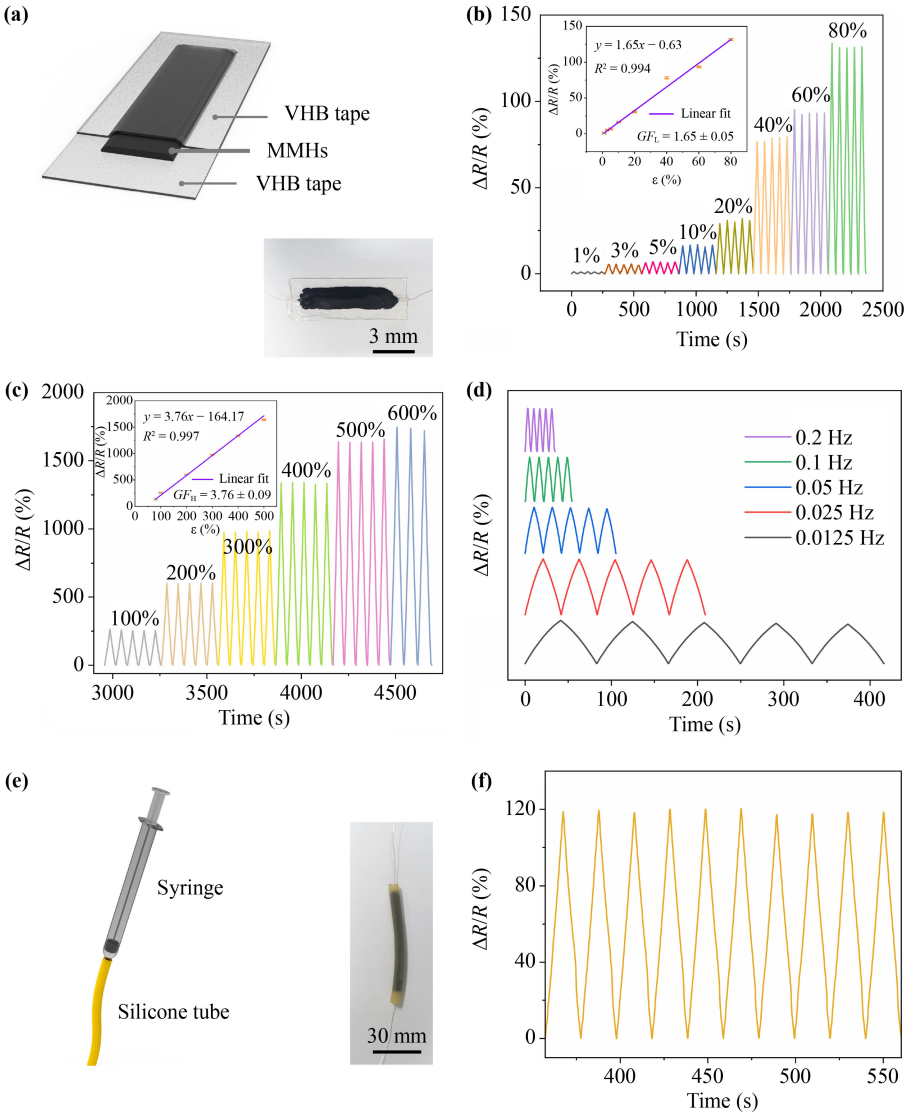

Fig. 2 MMHs-based tensile strain sensors and their performance. **(a)** Illustration of the sandwich structure of the MMHs-based strain sensor. The inset is an optical image of the sandwich strain sensor with two silver wires as electrodes. **(b, c)** Real-time relative resistance variation response of the sandwich strain sensor under different strain magnitude with a constant frequency of 0.05 Hz. The insets show the relative response versus strain. **(d)** The relative resistance variation response of the sandwich strain sensor under different strain frequencies with a constant strain magnitude of 50%. **(e)** Schematic of the fabrication method of the fiber strain sensor. The inset is an optical image of the fiber strain sensor with two silver wires as electrodes. **(f)** The relative resistance variation responses of the fiber strain sensor under strain with a magnitude of 50% and a frequency of 0.05 Hz.

were performed, and the scatters plot in the insets of Figs. 2(b) and (c) are average values with standard deviation. It shows that whether under small (1%–80%) or large (80%–500%) deformation, the relative resistance variation response of the sandwich strain sensor always maintains a linear relationship with ε. Although the sandwich sensor was not damaged under the strain of 600%, the testing error was too large to be retained. By fitting the slope of the $\Delta R/R_0 - \varepsilon$ curves, the GF could be estimated. The least-squares fitting results with high determination coefficient (R^2) showed that the GF for small deformation range (GF_{L}) and large deformation range (GF_{H}) were 1.65 ± 0.05 and 3.76 ± 0.09, respectively. The sensitivity of the MMHs-based sandwich strain sensor is higher than that of other reported strain sensors with hydrogel [38–40]. Furthermore, the corresponding resistance change of different stretch frequencies with a constant strain of 50% was tested. Figure 2(d) shows that the performance of the sandwich strain sensor has no significant change in the frequency range of 0.0125–0.2 Hz, which shows the fast and stable electromechanical property of MMHs. It is worth mentioning that the tensile machine used in experiments can only be set at a maximum frequency of 0.2 Hz.

Owning to the injectable property of MMHs, a fiber strain sensor could be quickly fabricated by injecting hydrogel into a silicone tube using a syringe, as shown in Fig. 2(e). Using the same experimental setup as the sandwich strain sensor, Fig. 2(f) and Movie S2 in the Supplementary show the strain sensitivity of the fiber strain sensor.

The testing results showed that the sandwich strain sensor could detect a wide strain range and perform well under different operating frequencies. In addition, MMHs and VHB tapes are flexible enough to be attached to human skin, which is promising to work as a wearable and flexible sensor detecting kinds of human motion. As shown in the insets of Figs. 3(a)–(d), the sandwich strain sensor was flexible enough to be attached to the skin of different parts of the human body. Figure 3(a) shows the relative resistance variation of the sandwich strain sensor corresponding to elbow bending with different degrees. Consistent with the tensile experiments, the more significant the elbow flexion, the larger the resistance variation. Periodic flexing movement of the finger joint is shown in Fig. 3(b). Figure 3(c) shows the measurement results of human walking, which can be used for gait detection and evaluation in medical rehabilitation. As shown in Fig. 3(d), the sandwich strain sensor could also be attached to the surface of the laryngeal prominence to detect swallowing. The output signal of the sandwich sensor for swallowing is almost periodic and distinctive. Using flexible sensors to measure the vibration of the human throat is a promising way to realize speech recognition [49–51], which would not be affected by ambient noise.

The dehydrated MMHs became too hard and brittle for strain sensing. Since both MXene and hydrogel are used for radionuclide adsorbents due to their large specific area, excellent hydrophilicity, and abundant active adsorption sites, it is interesting to investigate the adsorption capacity of MMHs for radionuclide. Bench experiments were conducted on the MMHs dried naturally to remove Sr^{2+} from the aqueous solution. Figure 4(a) shows the RE of Sr^{2+} as a function of the contact time (30, 60, 120, and 180 min). After ~ 60 min, the adsorption process reached equilibrium with a $RE > 80\%$. To understand the sorption process of Sr^{2+} in MMHs, the sorption kinetics was investigated by fitting the pseudo-first-order and pseudo-second-order kinetic model [52–54], which are described by

$$q_t = q_e(1 - e^{-k_1 t}), \tag{4}$$

$$\frac{t}{q_t} = \frac{1}{k_2 q_e^2} + \frac{t}{q_e}, \tag{5}$$

where q_t (mg/g) and q_e (mg/g) are the adsorption weight of Sr^{2+} ions per mass of MMHs at a sampling

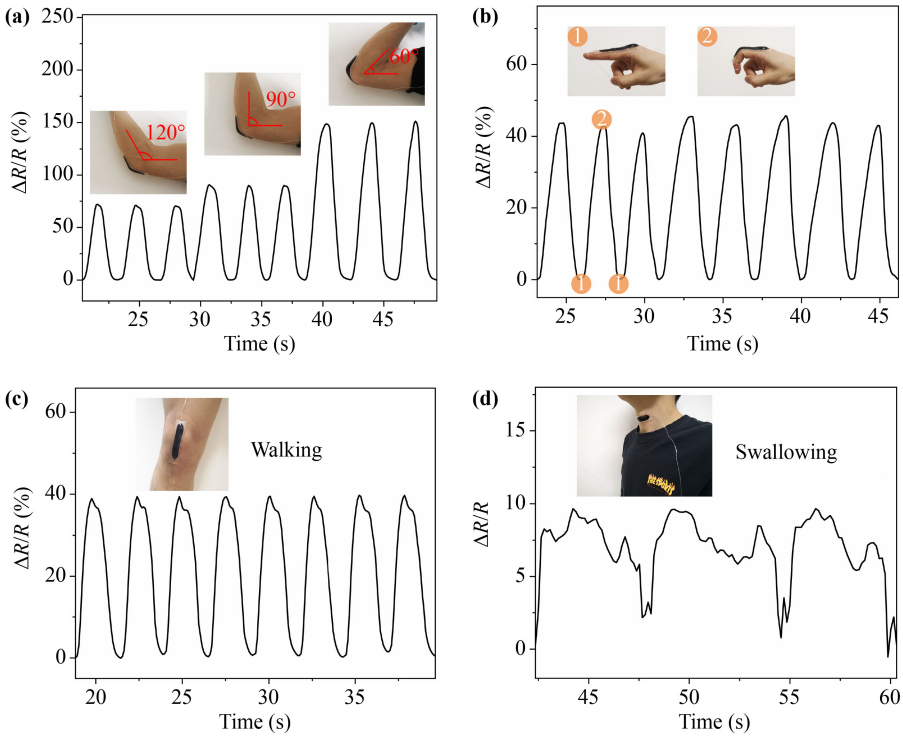

Fig. 3 Using flexible and wearable MMHs-based sandwich strain sensor to monitor various human motions. **(a–c)** Real-time relative resistance variation waveform corresponding to elbow bending with different angles, finger and knee joint bending, respectively. The insets show where the strain sensor was attached. **(d)** Real-time relative resistance variation waveform in response to swallowing.

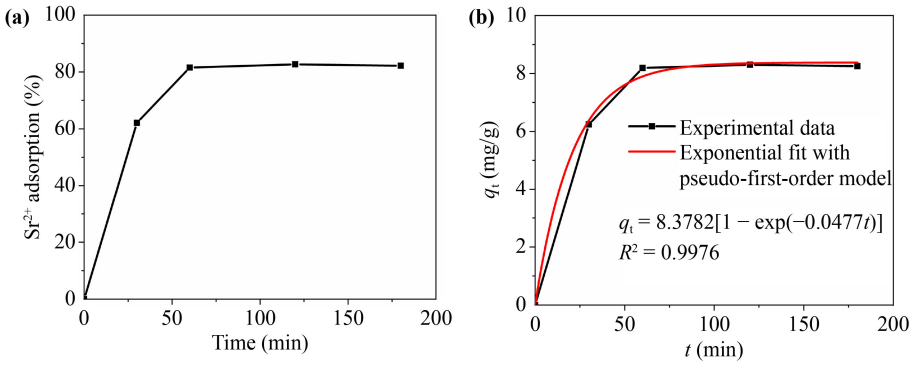

Fig. 4 Batch adsorption of Sr^{2+} ions onto the MMHs dried naturally. **(a)** Effects of contact time on the removal efficiency. **(b)** The time-dependent sorption pseudo-first-order kinetic plots.

Table 1 Kinetic parameters for Sr^{2+} adsorption onto MMHs described by the pseudo-first-order and pseudo-second-order models.

Pseudo-first-order model			Pseudo-second-order model		
k_1 (min^{-1})	q_e (mg/g)	R^2	k_2 ($g \cdot mg^{-1} \cdot min^{-1}$)	q_e (mg/g)	R^2
0.0477	8.3782	0.9976	0.0147	8.7032	0.9969

time and equilibrium, respectively; k_1 (min^{-1}) and k_2 (g/(mg·min)) are the adsorption rate constant of the pseudo-first-order and pseudo-second-order models, respectively. The pseudo-first-order model assumes that there is a large excess of one reactant so that its concentration could be treated as constant compared with the other reactant. The pseudo-second-order model assumes that the adsorption reaction is controlled by chemisorption. Table 1 summarizes the fitting results. Since the R^2 values for the two models were both larger than 0.99, the adsorption mechanism of Sr^{2+} ions in MMHs is attributed to both chemisorption or strong surface complexation reactions and mass transport. The fitting results of the pseudo-first-order model are shown in Fig. 4(b). The estimated q_e (8.38 mg/g) by the pseudo-first-order model was very close to the calculated q_e (8.25 mg/g) based on the experimental data.

4 Conclusions

In summary, multifunctional MMHs with a stable cross-linked structure were prepared by a bioinspired facile method. Attributed to the stable chelation between Ca^{2+} ions in ACC and reactive functional groups in both PAA and MXene nanosheets, the as-prepared MMHs showed outstanding stretchability, editability and self-healing ability. Water-rich MMHs showed excellent tensile strain sensitivity and can be used to fabricate flexible and wearable strain sensors, which showed a super-wide sensing range (1%–500%) with a maximum GF of 3.76 ± 0.09. The prepared strain sensor can be directly attached to the human skin surface to detect tiny and large human motions. Dehydrated MMHs can be used to remove Sr^{2+} from aqueous solutions. Batch experimental results suggested the highly efficient adsorption ability of MMHs for Sr^{2+} ions, and the maximum sorption can be attained within 60 min. This work showed the great potential of MMHs in strain sensing and radioactive wastewater treatment, which indicates the multifunctionality of MXene-based hydrogels.

Electronic supplementary materials are available in the online version of this article at https://doi.org/10.1007/s11467-022-1181-2 and https://journal.hep.com.cn/fop/EN/10.1007/s11467-022-1181-2 and are accessible for authorized users.

Declaration of competing interest There are no conflicts of interest to declare.

Acknowledgements This work was financially supported by the Fundamental Research Funds for Central Universities and also supported by the National Key R&D Program of China (Grant No. 2016YFC1402504).

References

1. F. Nudelman and N. A. J. M. Sommerdijk, Biomineralization as an inspiration for materials chemistry, *Angew. Chem. Int. Ed.* 51(27), 6582 (2012)
2. M. A. Meyers, J. McKittrick, and P. Y. Chen, Structural biological materials: Critical mechanics-materials connections, *Science* 339(6121), 773 (2013)
3. L. Addadi, S. Raz, and S. Weiner, Taking advantage of disorder: Amorphous calcium carbonate and its roles in biomineralization, *Adv. Mater.* 15(12), 959 (2003)
4. S. Weiner, J. Mahamid, Y. Politi, Y. Ma, and L. Addadi, Overview of the amorphous precursor phase strategy in biomineralization, *Front. Mater. Sci. China* 3(2), 104 (2009)
5. S. Sun, L. B. Mao, Z. Lei, S. H. Yu, and H. Cölfen, Hydrogels from amorphous calcium carbonate and polyacrylic acid: Bio-inspired materials for "mineral plastics", *Angew. Chem. Int. Ed.* 55(39), 11765 (2016)

6. K. Y. Lee and D. J. Mooney, Hydrogels for tissue engineering, *Chem. Rev.* 101(7), 1869 (2001)
7. D. Buenger, F. Topuz, and J. Groll, Hydrogels in sensing applications, *Prog. Polym. Sci.* 37(12), 1678 (2012)
8. Y. S. Zhang and A. Khademhosseini, Advances in engineering hydrogels, *Science* 356(6337), eaaf3627 (2017)
9. Y. Tai, M. Mulle, I. Aguilar Ventura, and G. Lubineau, A highly sensitive, low-cost, wearable pressure sensor based on conductive hydrogel spheres, *Nanoscale* 7(35), 14766 (2015)
10. Z. Lei, Q. Wang, S. Sun, W. Zhu, and P. Wu, A bioinspired mineral hydrogel as a self-healable, mechanically adaptable ionic skin for highly sensitive pressure sensing, *Adv. Mater.* 29(22), 1700321 (2017)
11. S. Lin, Y. Zhong, X. Zhao, T. Sawada, X. Li, W. Lei, M. Wang, T. Serizawa, and H. Zhu, Synthetic multifunctional graphene composites with reshaping and self-healing features via a facile biomineralization-inspired process, *Adv. Mater.* 30(34), 1803004 (2018)
12. H. Zhang, J. Guo, Y. Wang, L. Sun, and Y. Zhao, Stretchable and conductive composite structural color hydrogel films as bionic electronic skins, *Adv. Sci. (Weinh.)* 8(20), 2102156 (2021)
13. C. Li, Towards conductive hydrogels in E-skins: A review on rational design and recent developments, *RSC Advances* 11(54), 33835 (2021)
14. W. Li, F. Gao, X. Wang, N. Zhang, and M. Ma, Strong and robust polyaniline-based supramolecular hydrogels for flexible supercapacitors, *Angew. Chem.* 128(32), 9342 (2016)
15. J. Zeng, L. Dong, W. Sha, L. Wei, and X. Guo, Highly stretchable, compressible and arbitrarily deformable all-hydrogel soft supercapacitors, *Chem. Eng. J.* 383, 123098 (2020)
16. C. Chang, W. Chen, Y. Chen, Y. Chen, Y. Chen, et al., Recent progress on two-dimensional materials, *Acta Phys. -Chim. Sin.* 37(12), 2108017 (2021)
17. L. Jin-Cheng, Z. Xu, and Z. Zhen, Recent advances in MXene: Preparation, properties, and applications, *Front. Phys.* 10, 3 (2015)
18. R. Qin, X. Li, M. Hu, G. Shan, R. Seeram, and M. Yin, Preparation of high-performance MXene/PVA-based flexible pressure sensors with adjustable sensitivity and sensing range, *Sens. Actuators A Phys.* 338, 113458 (2022)
19. R. Qin, G. Shan, M. Hu, and W. Huang, Two-dimensional transition metal carbides and/or nitrides (MXenes) and their applications in sensors, *Mater. Today Phys.* 21, 100527 (2021)
20. Q. Zhao, Y. Jiang, Z. Duan, Z. Yuan, J. Zha, Z. Wu, Q. Huang, Z. Zhou, H. Li, F. He, Y. Su, C. Tan, and H. Tai, A Nb_2CT_x/sodium alginate-based composite film with neuron-like network for self-powered humidity sensing, *Chem. Eng. J.* 438, 135588 (2022)
21. M. R. Lukatskaya, S. Kota, Z. Lin, M. Q. Zhao, N. Shpigel, M. D. Levi, J. Halim, P. L. Taberna, M. W. Barsoum, P. Simon, and Y. Gogotsi, Ultra-high-rate pseudocapacitive energy storage in two-dimensional transition metal carbides, *Nat. Energy* 2(8), 17105 (2017)
22. M. Hu, N. Zhang, G. Shan, J. Gao, J. Liu, and R. K. Y. Li, Two-dimensional materials: Emerging toolkit for construction of ultrathin high-efficiency microwave shield and absorber, *Front. Phys.* 13(4), 138113 (2018)
23. M. Naguib, M. Kurtoglu, V. Presser, J. Lu, J. Niu, M. Heon, L. Hultman, Y. Gogotsi, and M. W. Barsoum, Two-dimensional nanocrystals produced by exfoliation of Ti_3AlC_2, *Adv. Mater.* 23(37), 4248 (2011)
24. Y.-Z. Zhang, J. K. El-Demellawi, Q. Jiang, G. Ge, H. Liang, K. Lee, X. Dong, and H. N. Alshareef, MXene hydrogels: Fundamentals and applications, *Chem. Soc. Rev.* 49, 7229 (2020)
25. K. H. Lee, Y. Z. Zhang, H. Kim, Y. Lei, S. Hong, S. Wustoni, A. Hama, S. Inal, and H. N. Alshareef, Muscle fatigue sensor based on $Ti_3C_2T_x$ MXene hydrogel, *Small Methods* 5(12), 2100819 (2021)
26. Y. Zhang, K. Chen, Y. Li, J. Lan, B. Yan, L. Shi, and R. Ran, High-strength, self-healable, temperature-sensitive, MXene-containing composite hydrogel as a smart compression sensor, *ACS Appl. Mater. Interfaces* 11(50), 47350 (2019)
27. Y. Cai, J. Shen, C. W. Yang, Y. Wan, H. L. Tang, A. A. Aljarb, C. Chen, J. H. Fu, X. Wei, K. W. Huang, Y. Han, S. J. Jonas, X. Dong, and V. Tung, Mixed-dimensional MXene-hydrogel heterostructures for electronic skin sensors with ultrabroad working range, *Sci. Adv.* 6(48), eabb5367 (2020)
28. Y. Z. Zhang, K. H. Lee, D. H. Anjum, R. Sougrat, Q. Jiang, H. Kim, and H. N. Alshareef, MXenes stretch hydrogel sensor performance to new limits, *Sci. Adv.* 4(6), eaat0098 (2018)
29. J. Huang, X. Huang, and P. Wu, One stone for three birds: One-step engineering highly elastic and conductive hydrogel electronics with multilayer MXene as initiator, crosslinker and conductive filler simultaneously, *Chem. Eng. J.* 428, 132515 (2022)
30. S. K. Hwang, S. M. Kang, M. Rethinasabapathy, C. Roh, and Y. S. Huh, MXene: An emerging two-dimensional layered material for removal of radioactive pollutants, *Chem. Eng. J.* 397, 125428 (2020)
31. L. Wang, W. Tao, L. Yuan, Z. Liu, Q. Huang, Z. Chai, J. K. Gibson, and W. Shi, Rational control of the interlayer space inside two-dimensional titanium carbides for highly efficient uranium removal and imprisonment, *Chem. Commun. (Camb.)* 53(89), 12084 (2017)
32. B. M. Jun, C. M. Park, J. Heo, and Y. Yoon, Adsorption of Ba^{2+} and Sr^{2+} on $Ti_3C_2T_x$ MXene in model fracking wastewater, *J. Environ. Manage.* 256, 109940 (2020)
33. S. Li, L. Wang, J. Peng, M. Zhai, and W. Shi, Efficient thorium (IV) removal by two-dimensional Ti_2CT_x MXene from aqueous solution, *Chem. Eng. J.* 366, 192 (2019)
34. M. Khan and I. M. C. Lo, A holistic review of hydrogel applications in the adsorptive removal of aqueous pollutants: Recent progress, challenges, and perspectives, *Water Res.* 106, 259 (2016)
35. C. Zhao, L. Hu, C. Zhang, S. Wang, X. Wang, and Z. Huo, Preparation of biochar-interpenetrated iron-alginate hydrogel as a PH-independent sorbent for removal of Cr(VI) and Pb(II), *Environ. Pollut.* 287, 117303 (2021)
36. Z. Wang, T. T. Li, H. K. Peng, H. T. Ren, C. W. Lou, and J. H. Lin, Low-cost hydrogel adsorbent enhanced

by trihydroxy melamine and β-cyclodextrin for the removal of Pb(II) and Ni(II) in water, *J. Hazard. Mater.* 411, 125029 (2021)
37. H. Mittal, A. Al Alili, and S. M. Alhassan, Adsorption isotherm and kinetics of water vapors on novel superporous hydrogel composites, *Microporous Mesoporous Mater.* 299, 110106 (2020)
38. V. Van Tran, D. Park, and Y. C. Lee, Hydrogel applications for adsorption of contaminants in water and wastewater treatment, *Environ. Sci. Pollut. Res. Int.* 25(25), 24569 (2018)
39. M. Le Flem, X. Liu, S. Doriot, T. Cozzika, and I. Monnet, Irradiation damage in $Ti_3(Si, Al)C_2$: A TEM investigation, *Int. J. Appl. Ceram. Technol.* 7(6), 766 (2010)
40. C. Wang, T. Yang, S. Kong, J. Xiao, J. Xue, Q. Wang, C. Hu, Q. Huang, and Y. Wang, Effects of He irradiation on Ti3AlC2: Damage evolution and behavior of He bubbles, *J. Nucl. Mater.* 440(1-3), 606 (2013)
41. H. Liu, X. Chen, Y. Zheng, D. Zhang, Y. Zhao, C. Wang, C. Pan, C. Liu, and C. Shen, Lightweight, superelastic, and hydrophobic polyimide nanofiber/MXene composite aerogel for wearable piezoresistive sensor and oil/water separation applications, *Adv. Funct. Mater.* 31(13), 2008006 (2021)
42. M. Tian, X. Chen, S. Sun, D. Yang, and P. Wu, A bioinspired high-modulus mineral hydrogel binder for improving the cycling stability of microsized silicon particle-based lithium-ion battery, *Nano Res.* 12(5), 1121 (2019)
43. J. Yan, J. Zhu, M. Cui, J. Zhang, F. Ma, Y. Su, and X. Han, Multifunctional mineral hydrogels: Potential in artificially intelligent skins and drug delivery, *ACS Omega* 4(21), 19145 (2019)
44. D. Gebauer, P. N. Gunawidjaja, J. Y. P. Ko, Z. Bacsik, B. Aziz, L. Liu, Y. Hu, L. Bergström, C. W. Tai, T. K. Sham, M. Edén, and N. Hedin, Proto-calcite and proto-vaterite in amorphous calcium carbonates, *Angew. Chem. Int. Ed.* 49(47), 8889 (2010)
45. J. Li, R. Qin, L. Yan, Z. Chi, Z. Yu, N. Li, M. Hu, H. Chen, and G. Shan, Plasmonic light illumination creates a channel to achieve fast degradation of $Ti_3C_2T_x$ nanosheets, *Inorg. Chem.* 58(11), 7285 (2019)
46. G. Cai, J. Wang, K. Qian, J. Chen, S. Li, and P. S. Lee, Extremely stretchable strain sensors based on conductive self-healing dynamic cross-links hydrogels for human-motion detection, *Adv. Sci. (Weinh.)* 4(2), 1600190 (2017)
47. S. Lin, X. Zhao, X. Jiang, A. Wu, H. Ding, Y. Zhong, J. Li, J. Pan, B. Liu, and H. Zhu, Highly stretchable, adaptable, and durable strain sensing based on a bioinspired dynamically cross-linked graphene/polymer composite, *Small* 15(19), 1900848 (2019)
48. Y. J. Liu, W. T. Cao, M. G. Ma, and P. Wan, Ultrasensitive wearable soft strain sensors of conductive, self-healing, and elastic hydrogels with synergistic "soft and hard" hybrid networks, *ACS Appl. Mater. Interfaces* 9(30), 25559 (2017)
49. S. Lee, J. Kim, I. Yun, G. Y. Bae, D. Kim, S. Park, I. M. Yi, W. Moon, Y. Chung, and K. Cho, An ultrathin conformable vibration-responsive electronic skin for quantitative vocal recognition, *Nat. Commun.* 10(1), 2468 (2019)
50. Y. H. Jung, S. K. Hong, H. S. Wang, J. H. Han, T. X. Pham, H. Park, J. Kim, S. Kang, C. D. Yoo, and K. J. Lee, Flexible piezoelectric acoustic sensors and machine learning for speech processing, *Adv. Mater.* 32(35), 1904020 (2020)
51. R. Qin, M. Hu, X. Li, T. Liang, H. Tan, J. Liu, and G. Shan, A new strategy for the fabrication of a flexible and highly sensitive capacitive pressure sensor, *Microsyst. Nanoeng.* 7(1), 100 (2021)
52. J. P. Simonin, On the comparison of pseudo-first order and pseudo-second order rate laws in the modeling of adsorption kinetics, *Chem. Eng. J.* 300, 254 (2016)
53. J. Liang, J. Li, X. Li, K. Liu, L. Wu, and G. Shan, The sorption behavior of CHA-type zeolite for removing radioactive strontium from aqueous solutions, *Separ. Purif. Tech.* 230, 115874 (2020)
54. N. J. Coleman, D. S. Brassington, A. Raza, and A. P. Mendham, Sorption of Co^{2+} and Sr^{2+} by waste-derived 11 Å tobermorite, *Waste Manag.* 26(3), 260 (2006)